



# Correlation of the catalytic performance with Nb<sub>2</sub>O<sub>5</sub> surface properties in the hydrodeoxygenation of lignin model compound

Yu Xin<sup>a</sup>, Lin Dong<sup>a</sup>, Yong Guo<sup>a,\*</sup>, Xiaohui Liu<sup>a</sup>, Yongfeng Hu<sup>b</sup>, Yanqin Wang<sup>a,\*</sup>

<sup>a</sup> Shanghai Key Laboratory of Functional Materials Chemistry, Research Institute of Industrial Catalysis, School of Chemistry and Molecular Engineering, East China University of Science and Technology, Shanghai 200237, China

<sup>b</sup> Canadian Light Source Inc., 44 Innovation Boulevard, Saskatoon, SK S7N 2V3, Canada

## ARTICLE INFO

### Article history:

Received 10 August 2018

Revised 10 April 2019

Accepted 4 May 2019

### Keywords:

Lignin  
4-methylphenol  
Hydrodeoxygenation  
Aromatic hydrocarbons  
Ru/Nb<sub>2</sub>O<sub>5</sub>  
Raman  
XANES  
DRIFTS  
Py-IR

## ABSTRACT

Production of aromatic hydrocarbons through lignin hydrodeoxygenation (HDO) is of significant importance. Previously, we found that Ru/Nb<sub>2</sub>O<sub>5</sub> was an excellent catalyst for the conversion of lignin to arenes with relatively high selectivity (71%). Herein, we aim to clarify which properties of Nb<sub>2</sub>O<sub>5</sub> influence the activity and selectivity. Four Ru/Nb<sub>2</sub>O<sub>5</sub> catalysts with different Nb<sub>2</sub>O<sub>5</sub> morphologies were used in the HDO of 4-methylphenol. Intensive studies show that layered Nb<sub>2</sub>O<sub>5</sub> supported Ru has more Nb=O groups (unsaturated NbO<sub>x</sub> sites) and highest Ru dispersion, which led to the highest activity and toluene selectivity, this was further confirmed by loading pre-synthesized Ru colloids in various Nb<sub>2</sub>O<sub>5</sub>. Finally, a Ru/Nb<sub>2</sub>O<sub>5</sub> catalyst with more unsaturated Nb=O groups was designed and it was found that even with enzymatic lignin as the feedstock, the selectivity to arenes can reach up to 94.8% with the yield of hydrocarbons of 99.6%. This study provides a promising strategy for catalyst design towards the selective production of aromatic hydrocarbons from lignin.

© 2019 Elsevier Inc. All rights reserved.

## 1. Introduction

Lignin is a heterogeneous aromatic biopolymer that accounts for 15–35% of the mass of lignocellulosic biomass and is the only large quantity of natural aromatic sources; therefore, its transformation to chemicals and fuels has received increasing attention [1–5]. Various strategies have been developed for lignin valorization, for example, the depolymerization of lignin into low-molecular-weight feedstocks under mild conditions followed by sequential upgrading to useful chemicals and fuels [6–16]. However, retaining the aromatic functionality while selectively cleaving C–O bonds, especially the C<sub>aromatic</sub>–O in phenol unit, is critical but extremely challenging for the conversion of lignin into aromatic hydrocarbons [5]. Aromatic hydrocarbons are not only important feedstocks of basic organic chemicals, but also the important blend of jet fuels because of its high volume density as well as the property to prevent leaking of jet fuels from aging rubber rings [17]. Therefore, the investigation on enhancing aromatic

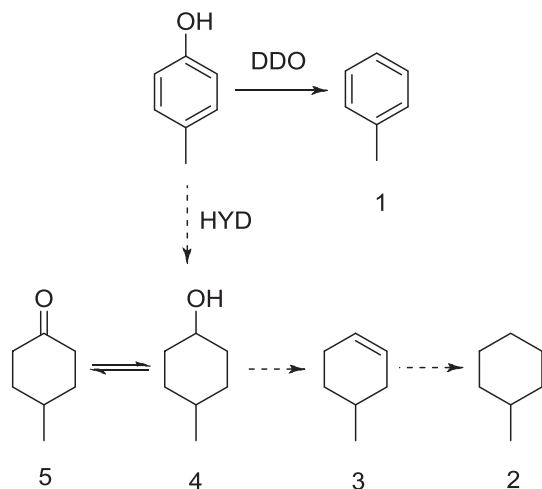
hydrocarbons' selectivity and productivity during hydrodeoxygenation (HDO) of lignin is necessary and urgent.

Normally, aromatic hydrocarbons produced from phenols (components of bio-oils and model compounds of lignin) undergo via two major reaction pathways (Scheme 1) [18–20]: (1) the direct deoxygenation to benzene (DDO path); and (2) the hydrogenation of phenols to cyclohexanone and cyclohexanol, followed by dehydration to cyclohexene and further dehydrogenation to benzene (HYD path). However, these two routes are always accompanied with the hydrogenation of aromatic rings or cyclohexene, leading to the formation of cyclohexane. Previous report [19] proved that it is dramatically difficult to produce aromatic hydrocarbons with high selectivity owing to the high dissociation energy of C<sub>aromatic</sub>–O bond and excessive hydrogenation of aromatic ring.

Recently, Nb<sub>2</sub>O<sub>5</sub> supported Ru catalysts were proved to be excellent for the hydrodeoxygenation of lignin and model compounds to aromatic hydrocarbons due to the synergistic effects between Ru and Nb<sub>2</sub>O<sub>5</sub> [21]. The selectivity to aromatic hydrocarbons reached 71% with the total conversion of lignin monomers. Inelastic neutron scattering (INS) and DFT calculation showed that NbO<sub>x</sub> species have significant promotional effect on the cleavage of C–O bond, which is attributed to the strong adsorption of phenol on NbO<sub>x</sub> species and the reduction of the dissociation energy of C–O

\* Corresponding authors.

E-mail addresses: [guoyong@ecust.edu.cn](mailto:guoyong@ecust.edu.cn) (Y. Guo), [wangyanqin@ecust.edu.cn](mailto:wangyanqin@ecust.edu.cn) (Y. Wang).



**Scheme 1.** Proposed reaction pathway of the hydrodeoxygenation (HDO) of 4-methylphenol.

bonds. In addition, another Nb-based catalyst, Ru/Nb<sub>2</sub>O<sub>5</sub>-SiO<sub>2</sub> also exhibited good activity and selectivity in the HDO of lignin model compounds with 2-PrOH as a hydrogen source through DDO pathway [22].

As supported metal catalyst, both of the metal particle size and support morphology would play important roles in activity and selectivity in various reactions, including the HDO of lignin model compound. It is reported that metal particle size has obvious effect on the reactivity and selectivity in many reactions [23–26]. For example, Ru nanoparticles highly dispersed on TiO<sub>2</sub> [25] or NbOPO<sub>4</sub> [26] has high activity and selectivity in the HDO of phenol or the hydrogenolysis of 2-(2-methoxyphenoxy)-1-phenylethanol following with phenol HDO. In addition, the morphology of oxides and oxide support also affects the activity and selectivity for many reactions [27–30]. For example, Noronha et al. [29] reported that the difference in the density of oxophilic sites in three types of zirconia supported Pd catalysts, which was caused by morphology, resulted in significantly different activity and selectivity in the HDO of phenol. Tsang et al. [30] found that nanostructured Nb<sub>2</sub>O<sub>5</sub> materials with high surface area and large amounts of Lewis acid sites exhibited superior performance in glucose conversion compared to other bulk Nb<sub>2</sub>O<sub>5</sub>.

Based on above description, it is speculated that the different morphologies of Nb<sub>2</sub>O<sub>5</sub> supports may affect the activity and/or selectivity in the HDO of lignin and its model compounds over Ru/Nb<sub>2</sub>O<sub>5</sub> catalysts. The understanding of the relationships between the properties of Nb<sub>2</sub>O<sub>5</sub> and the catalytic performance will help us to design a more active HDO catalyst. Herein, four types of Nb<sub>2</sub>O<sub>5</sub> with different morphologies were synthesized and used to evaluate their activity and selectivity in the HDO of lignin-derived compound, 4-methylphenol after impregnation with Ru. It is revealed that the layered Nb<sub>2</sub>O<sub>5</sub> supported Ru catalyst showed the highest activity and selectivity to toluene, which may be due to its high surface area, the unsaturated state of Nb<sub>2</sub>O<sub>5</sub> and high dispersion of Ru. Moreover, in order to investigate the intrinsic effect of Ru nanoparticles and Nb<sub>2</sub>O<sub>5</sub> supports, colloidal Ru nanocrystals with uniform size distribution were also synthesized and supported on various Nb<sub>2</sub>O<sub>5</sub>. Combined with Raman, XANES, DRIFTS and Py-IR characterizations, it showed that the activity was influenced by the coordination states of Nb, while the size of Ru nanoparticles affected the selectivity to toluene. Furthermore, another layered Nb<sub>2</sub>O<sub>5</sub> with more unsaturated Nb=O groups was prepared and used as Ru support for the HDO of 4-methylphenol and enzymatic lignin. As expected, a high mole yield of C<sub>7</sub>~C<sub>9</sub>

hydrocarbons (99.6%) with as high as 94.8% selectivity to C<sub>7</sub>~C<sub>9</sub> aromatic hydrocarbons was obtained from enzymatic lignin.

## 2. Experimental section

### 2.1. Chemicals

All chemicals used here were purchased from Sinopharm Chemical Reagent Co. Ltd, except for RuCl<sub>3</sub> and 4-methylphenol, which were purchased from Aladdin Reagent Co. Ltd. All purchased chemicals were of analytical grade and used without further purification. The enzymatic lignin (composition see Table S1) was obtained from ShanDong Longli Co. Ltd.

### 2.2. Catalyst preparation

The Nb precursors (niobium citrate and niobium oxalate), with an Nb concentration of 0.4 mol L<sup>-1</sup>, were prepared according to the literature [31].

The Nb<sub>2</sub>O<sub>5</sub> flowers (denoted as F-Nb<sub>2</sub>O<sub>5</sub>) were synthesized according to literature [32]. Typically, 0.4 g (1.48 mmol) of NbCl<sub>5</sub> was first dissolved in 4 mL ethanol under vigorous stirring, then 17 mL H<sub>2</sub>O and 3 mL ammonia were added into the above solution. After the mixture was aged for 2 h at ambient temperature, the precipitates were centrifuged and transferred to a 100 mL Teflon-lined stainless-steel autoclave pre-charged with 56 mL deionized water. The hydrothermal treatment was performed under 200 °C for 24 h. Finally, the resulting precipitates were collected, filtered, washed with deionized water and dried at 80 °C for 24 h; followed by calcination in air at 600 °C for 2 h with a linear heating ramp of 3 °C min<sup>-1</sup>.

The hollowed Nb<sub>2</sub>O<sub>5</sub> (denoted as H-Nb<sub>2</sub>O<sub>5</sub>) was synthesized according to literature with modification [33]. Typically, 1.37 g of resorcinol, 2.02 g of formaldehyde and 9.60 g of niobium oxalate were dissolved in 50 mL deionized water and stirred for 4 h at 40 °C, then the solution was transferred to a 100 mL Teflon-lined stainless-steel autoclave and heated at 180 °C for 24 h. After reaction, the solid was separated by filtration, then washed with distilled water, dried at 50 °C for 24 h, followed by calcination in air at 600 °C for 2 h with a linear heating ramp of 3 °C min<sup>-1</sup>.

The mesoporous Nb<sub>2</sub>O<sub>5</sub> (denoted as M-Nb<sub>2</sub>O<sub>5</sub>) was synthesized according to our previous report [31]. Typically, 1.00 g of CTAB was dissolved in 15 mL H<sub>2</sub>O at 35 °C, then 40 mL niobium tartrate was dropped into the above solution with continuous stirring. After stirred at 35 °C for 1 h, the mixture was aged in a Teflon-lined stainless-steel autoclave for 24 h at 160 °C. The resulting precipitates were collected, filtered, washed with deionized water and dried at 50 °C for 24 h, followed by calcination in air at 500 °C for 5 h with a linear heating ramp of 1 °C min<sup>-1</sup>.

The layered Nb<sub>2</sub>O<sub>5</sub> (denoted as L3-Nb<sub>2</sub>O<sub>5</sub>) was synthesized by changing the substrates and reaction condition following Murayama's work [34]. In a typical process, 19.20 g of self-prepared niobium oxalate and 0.71 g of ammonium oxalate were dissolved in 50 mL deionized water and sealed in a 100 mL Teflon-lined autoclave. After being treated with hydrothermal method at 180 °C for 3 days, calcination at 400 °C was lasted for 4 h under air with a linear heating ramp of 10 °C min<sup>-1</sup>.

Incipient wetness method was used to prepare Ru/Nb<sub>2</sub>O<sub>5</sub>(WI) catalysts. Typically, an aqueous solution of RuCl<sub>3</sub> was mixed with various Nb<sub>2</sub>O<sub>5</sub> support and stirred to be slurry, then the slurry was dried at 60 °C for 12 h. The samples were reduced in a flow of 10% H<sub>2</sub>/Ar at 400 °C for 4 h (3 °C min<sup>-1</sup>) and then purged with N<sub>2</sub> for 1 h until to room temperature. After that, the sample was taken out without passivation and directly transferred into the autoclave reactor. The initial loading of Ru was 2.0 wt% in all cases.

Ru/Nb<sub>2</sub>O<sub>5</sub> (NP) catalysts were prepared through adsorption of colloidal Ru NPs on the Nb<sub>2</sub>O<sub>5</sub> supports. Colloidal Ru NPs with different sizes were prepared by the reduction of RuCl<sub>3</sub> with ascorbic acid in the aqueous phase at 80 °C for 1 min, 5 min and 12 h, respectively, according to previous report [35]. Then the Nb<sub>2</sub>O<sub>5</sub> support was added into the Ru NPs colloidal solution and stirred for 24 h. After that, the sample was centrifuged, washed with deionized water, dried at 50 °C in a vacuum oven, and calcined at 300 °C for 4 h under N<sub>2</sub> atmosphere.

### 2.3. Characterization

The powder XRD patterns were recorded with a Rigaku D/max-2550VB/PC diffractometer by using Cu K $\alpha$  ( $L = 0.15406$  nm) radiation that was operated at 40 kV and 40 mA.

The N<sub>2</sub> adsorption-desorption isotherms were measured at –196 °C using a Micromeritics ASAP 2020 M sorption analyzer. The BET method was used to calculate the specific surface area.

The transmission electron microscopy (TEM) was performed on a JEOL 2100 electron microscope that was operated at 200 kV.

The actual Ru loading in the sample was detected by inductively coupled plasma-atomic emission spectroscopy (ICP-AES) on a Perkin-Elmer Optima 2100 DV spectrometer.

Raman spectra were recorded on a Renishaw Raman spectrometer under ambient conditions, and the 514 nm line of the Spectra Physics Ar<sup>+</sup> laser was used as the excitation wavelength. The laser beam intensity and spectrum slit width was 2mW and 3.5 cm<sup>-1</sup>, respectively. X-ray absorption near edge structure (XANES) measurement was conducted at the Canadian Light Source using the Soft X-ray Microcharacterization Beamline with a selected energy window (e.g. Nb L $\alpha$  for Nb L3-edge). A four-element Si drift solid state detector was equipped for the fluorescence yield measurement.

H<sub>2</sub> temperature-programmed reduction (H<sub>2</sub>-TPR) measurements of the catalysts were conducted using an apparatus (PX200, Tianjin Golden Eagle Technology Co. Ltd). 50 mg sample was directly heated from room temperature to 400 °C at a rate of 10 °C/min in a flow of 10 vol% H<sub>2</sub>/Ar (40 mL/min). The hydrogen consumption was monitored using a thermal conductivity detector (TCD).

Infrared (IR) spectra of pyridine adsorption were recorded on NICOLET iS50 FT-IR spectrometer, with 32 scans at an effective resolution of 4 cm<sup>-1</sup>. The samples were pressed into self-supporting disks and placed in an IR cell. The disk was dehydrated by heating at 400 °C for 1 h under vacuum. After the cell was cooled to room temperature, the IR spectrum was recorded as background. Pyridine vapor was then introduced into the cell at room-temperature until equilibrium was reached, and then a second spectrum was recorded. Then evacuation was performed at 100 °C for 10 min followed by spectral acquisitions.

Diffuse Reflectance Infrared Fourier Transform Spectroscopy (DRIFTS) was collected with a NICOLET iS50 FT-IR spectrometer equipped with an MCT/A detector. Firstly, the catalysts (0.05 g) were in situ reduced in the cell in H<sub>2</sub> at 400 °C for 30 min and cooled to 35 °C in N<sub>2</sub>, and a background was recorded. The reduction time decreases to 30 min due to the small amount of catalyst. Then 4-methylphenol with N<sub>2</sub> was bubbled into the cell for 30 min, blowing with N<sub>2</sub> for 60 min. Finally, the temperature was increased from 35 to 150 and 200 °C, respectively and the adsorption spectra of 4-methylphenol were recorded at different time.

The Ru dispersion was measured by CO chemisorption using the dynamic adsorption method with an automatic chemisorbent (ChemiSorb 2720). Before adsorption, the samples (0.1 g) were reduced under pure H<sub>2</sub> (60 mL/min) at 473 K for 30 min (10 K/min), cooled to room temperature, and flushed in He for 30 min. Then, pulses of 5% CO in He were injected until saturation was

reached, as monitored by a thermal conductivity detector (TCD). The Ru dispersion was calculated assuming a stoichiometry of 1:1 for CO adsorbed on Ru.

### 2.4. Catalysts test and products analysis

Typically, catalyst (0.04 g) and 4-methylphenol (0.2 g) were loaded into a 50 mL stainless autoclave reactor (Anhui Kemi Machinery Technology Co., Ltd) with water (15 mL) as the solvent. After the reactor was purged with H<sub>2</sub> for three times, 0.5 MPa H<sub>2</sub> was charged. Then the reaction was conducted at 250 °C with the magnetic stirring (600 r.p.m) and kept for a certain reaction time. The stirring speed of 600 r/min was sufficient for mass transfer (Fig. S3). After reaction, the reactor was quenched to ambient temperature in a water bath. The reaction mixture was extracted with ethyl acetate (10 g), followed by centrifugation to separate the solid catalyst. The organic phase was qualitatively analyzed using a GC-MS (Agilent 7890A–5975C) equipped with an HP-5 column and quantitatively analyzed by GC-FID (Agilent 7890A). Tridecane was taken as the internal standard. Both of the experiments and catalyst preparations were repeated three times. The number of conversion and yield were obtained by taking the average of three measurements.

## 3. Results and discussions

### 3.1. Characterization of the catalysts

Fig. 1 shows the XRD patterns of various Ru/Nb<sub>2</sub>O<sub>5</sub> (WI) catalysts. For sample L3-Nb<sub>2</sub>O<sub>5</sub>, only two diffraction peaks at 22.7° and 46.2° were observed obviously, indicating its layered structure and low degree of crystallinity [34]. M-Nb<sub>2</sub>O<sub>5</sub> sample displayed the structural characteristics of hexagonal Nb<sub>2</sub>O<sub>5</sub> (TT phase). The TT phase showed a low degree of crystallinity, which can be regarded as a modification of the orthorhombic T phase. For the samples of H-Nb<sub>2</sub>O<sub>5</sub> and F-Nb<sub>2</sub>O<sub>5</sub>, the peaks at 28.4° and 36.7° were split into two peaks, respectively, indicating the transformation from the pseudo-hexagonal TT phase to the orthorhombic T phase [36]. The sharp peaks for both of H-Nb<sub>2</sub>O<sub>5</sub> and F-Nb<sub>2</sub>O<sub>5</sub> samples indicate that they are highly crystallized. Additionally, no diffraction peaks corresponded to Ru were detected on M-Nb<sub>2</sub>O<sub>5</sub> and L3-Nb<sub>2</sub>O<sub>5</sub> catalysts and only a very broad peak at 42.7° corresponded to Ru is observed in the XRD patterns of H-Nb<sub>2</sub>O<sub>5</sub> and F-Nb<sub>2</sub>O<sub>5</sub> (Fig. 1B). These indicate the different particle sizes of Ru on different Nb<sub>2</sub>O<sub>5</sub>, but all are highly dispersed.

The TEM images of four Ru/Nb<sub>2</sub>O<sub>5</sub>(WI) catalysts are presented in Fig. 2. The Ru nanoparticles are anchored on F-Nb<sub>2</sub>O<sub>5</sub> (Fig. 2A) and H-Nb<sub>2</sub>O<sub>5</sub> (Fig. 2B) hosts and have a mean distribution of 7.6 nm and 1.9 nm, respectively, while it cannot be seen Ru nanoparticles on M-Nb<sub>2</sub>O<sub>5</sub> (Fig. 2C) and L3-Nb<sub>2</sub>O<sub>5</sub> (Fig. 2D). EDS-mapping analysis of Ru/M-Nb<sub>2</sub>O<sub>5</sub> and Ru/L3-Nb<sub>2</sub>O<sub>5</sub> show the presence of Ru on Nb-based supports homogeneously. It is consistent with the results from XRD and TEM, i.e. small Ru particles highly dispersed on four Ru/Nb<sub>2</sub>O<sub>5</sub> (WI).

Nitrogen sorption was carried out to measure the surface area of all Nb<sub>2</sub>O<sub>5</sub> supports and Ru/Nb<sub>2</sub>O<sub>5</sub> catalysts, the data were summarized in Table 1. It is found that after loading of Ru, all surface areas decreased, but in less extent. L3-Nb<sub>2</sub>O<sub>5</sub> and Ru/L3-Nb<sub>2</sub>O<sub>5</sub> had the highest surface area (197/181 m<sup>2</sup>·g<sup>-1</sup>), followed with M-Nb<sub>2</sub>O<sub>5</sub>/Ru/M-Nb<sub>2</sub>O<sub>5</sub> (50/44 m<sup>2</sup>·g<sup>-1</sup>) and H-Nb<sub>2</sub>O<sub>5</sub>/Ru/H-Nb<sub>2</sub>O<sub>5</sub> (42/36 m<sup>2</sup>·g<sup>-1</sup>). The surface areas of F-Nb<sub>2</sub>O<sub>5</sub> and Ru/F-Nb<sub>2</sub>O<sub>5</sub> are least, 16 and 15 m<sup>2</sup>·g<sup>-1</sup>, respectively. These four Nb<sub>2</sub>O<sub>5</sub> supports were prepared by adding different organic agents. Hexadecyl trimethyl ammonium bromide (CTAB) was used for M-Nb<sub>2</sub>O<sub>5</sub>, phenolic resin for H-Nb<sub>2</sub>O<sub>5</sub>, ammonium oxalate for L-Nb<sub>2</sub>O<sub>5</sub> and no

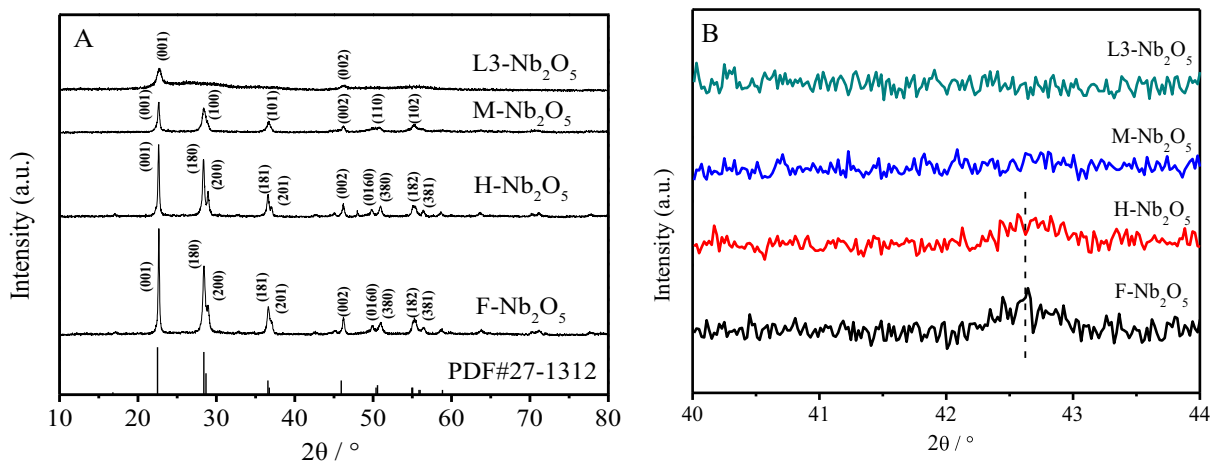


Fig. 1. XRD patterns of various Ru/Nb<sub>2</sub>O<sub>5</sub> (WI) catalysts.

template agent for F-Nb<sub>2</sub>O<sub>5</sub>, the organic agents played a significant role in the morphology control and led to different surface area.

The amount and dispersion of Ru in all four catalysts were measured by ICP and CO-pulse titration, and presented in Table 1. It is found that the amount of Ru is very close to the initial Ru loading, while the dispersion of Ru is different for these four catalysts. Layered Nb<sub>2</sub>O<sub>5</sub> supported Ru catalyst (Ru/L3-Nb<sub>2</sub>O<sub>5</sub> (WI)) had very high Ru dispersion (77%), while that of Ru/F-Nb<sub>2</sub>O<sub>5</sub> (WI) was extremely low (4.2%). The Ru dispersion in Ru/H-Nb<sub>2</sub>O<sub>5</sub> (WI) and Ru/M-Nb<sub>2</sub>O<sub>5</sub> (WI) was in the middle, 27% and 40.2%, respectively, indicating that Ru particles were well-dispersed on them. It can be seen that Ru dispersion positively correlated with the specific surface area of Nb<sub>2</sub>O<sub>5</sub>, i.e. the Ru nanoparticles exhibited smaller size with the increase of specific surface area, it is also in agreement with XRD results. However, the Ru particle size calculated from CO-pulse adsorption is large than that calculated from TEM images, especially for Ru/F-Nb<sub>2</sub>O<sub>5</sub> (WI) (Table S2). The inconsistency over F-Nb<sub>2</sub>O<sub>5</sub> may be caused by the inhomogeneity (co-existence of a little amount of large particles with small particles), as TEM image shown in Fig. S1.

The H<sub>2</sub>-TPR profiles of these four catalysts were presented in Fig. 3. It is shown that the reduction temperature of RuO<sub>x</sub> in the four catalysts increased in the following order: L3-Nb<sub>2</sub>O<sub>5</sub> < M-Nb<sub>2</sub>O<sub>5</sub> ≈ H-Nb<sub>2</sub>O<sub>5</sub> < F-Nb<sub>2</sub>O<sub>5</sub>, centered at 130, 147, 148 and 170 °C, respectively. This is consistent with the Ru dispersion in the catalysts, because it is usually considered that the lower reduction temperature was attributed to the high dispersion of smaller Ru particle size. Additionally, the TPR profiles of all the samples show a shoulder before the main reduction peak, it may associate with the smaller sized Ru nanoparticles due to the relative broad size distribution. For Ru/H-Nb<sub>2</sub>O<sub>5</sub> and Ru/M-Nb<sub>2</sub>O<sub>5</sub> samples, the difference of reduction temperature is not obvious, but from Ru dispersion and HRTEM, we can speculate that smaller Ru particles account for higher proportion on M-Nb<sub>2</sub>O<sub>5</sub>. It is worth noting that, there is no reduction peak for bare L3-Nb<sub>2</sub>O<sub>5</sub> support even at 500 °C (Fig. S2), but for Ru/L3-Nb<sub>2</sub>O<sub>5</sub>, an obviously new peak at high reduction temperature (310 °C) appears which could be attributed to the reduction of more stable ruthenium oxides that had strong interaction with layered Nb<sub>2</sub>O<sub>5</sub>.

### 3.2. HDO of 4-methylphenol over various Ru/Nb<sub>2</sub>O<sub>5</sub> (WI) catalysts

The catalytic activity and products distribution for the HDO of 4-methylphenol over different Ru/Nb<sub>2</sub>O<sub>5</sub> (WI) catalysts are depicted in Table 2. It is clear that the conversion and the products

distribution were dramatically different for different catalysts. Over Ru/F-Nb<sub>2</sub>O<sub>5</sub>, Ru/H-Nb<sub>2</sub>O<sub>5</sub> and Ru/M-Nb<sub>2</sub>O<sub>5</sub> catalysts, the conversion and selectivity to toluene were 21.2/54.9, 17.4/62.8 and 20.9/65.9, respectively. The main by-product was 4-methyl cyclohexanol, with the selectivity of 19.0, 15.2 and 17.8%, respectively. Excitingly, extremely high toluene selectivity (85.9%) was achieved over Ru/L3-Nb<sub>2</sub>O<sub>5</sub> catalyst, with 25.1% conversion of 4-methylphenol under the same reaction conditions. The difference was further confirmed by prolonging the reaction time (Table S3). The differences on conversion and selectivity to toluene may come from the difference of surface area of Nb<sub>2</sub>O<sub>5</sub> and Ru particle size with the exception of H-Nb<sub>2</sub>O<sub>5</sub>, in which the conversion is lower than expected, but the selectivity is in agreement with Ru particle size. We propose that Nb<sub>2</sub>O<sub>5</sub> would contribute to the activity, because it has been reported that the activation of C<sub>aromatic</sub>-O bonds happened over Nb<sub>2</sub>O<sub>5</sub> surface [21], while Ru particle size tuned the selectivity, the small sized Ru particles favor the hydrogenolysis of C-O bonds [26]. Ru/L3-Nb<sub>2</sub>O<sub>5</sub> catalyst has the highest surface area and Ru dispersion, resulting in the highest activity and selectivity. The other three catalysts have low surface area and Ru dispersion, making the competition of HYD route with DDO route more severely. Fig. S4 shows the profile of conversion rates/area and toluene production rates/area vs. surface area over four Nb-based catalysts and there is not constant or linear relationship. The exception for H-Nb<sub>2</sub>O<sub>5</sub> hints that there are other factors to affect the activity.

In order to investigate the intrinsic effect of Nb<sub>2</sub>O<sub>5</sub> supports, Ru colloids with particle size of 1.2 nm was pre-synthesized and loaded on these four Nb<sub>2</sub>O<sub>5</sub> supports (Fig. S5) to exclude the potential influence of Ru particle size. Such-prepared catalysts were denoted as Ru/Nb<sub>2</sub>O<sub>5</sub> (NP), and the Ru content of all samples confirmed by ICP was also similar (Table 3). The similar Ru diameters (1.1–1.3 nm) on four Nb<sub>2</sub>O<sub>5</sub> supports were determined with HRTEM and similar Ru dispersion (51.2–60.5%) were calculated from the average Ru particle size (Table S4). The catalytic activity and products' distribution for the HDO of 4-methylphenol over these four Ru/Nb<sub>2</sub>O<sub>5</sub> (NP) catalysts are summarized in Fig. 4 and Table 3. Notably, for the HDO of 4-methylphenol, the selectivity to toluene is not changed with the conversion, but remains nearly constant in the time courses. When fixed the size of Ru (NP, 1.2 nm), it is found that over all reaction times (from 0.5 h to 4 h), the conversion over different catalyst decreases in following order: Ru/L3-Nb<sub>2</sub>O<sub>5</sub> (NP) > Ru/F-Nb<sub>2</sub>O<sub>5</sub> (NP) ≈ Ru/M-Nb<sub>2</sub>O<sub>5</sub> (NP) > Ru/H-Nb<sub>2</sub>O<sub>5</sub> (NP). This sequence was the same as that over Ru/Nb<sub>2</sub>O<sub>5</sub> (WI) catalysts. Namely, Nb<sub>2</sub>O<sub>5</sub> with larger surface area exhi-

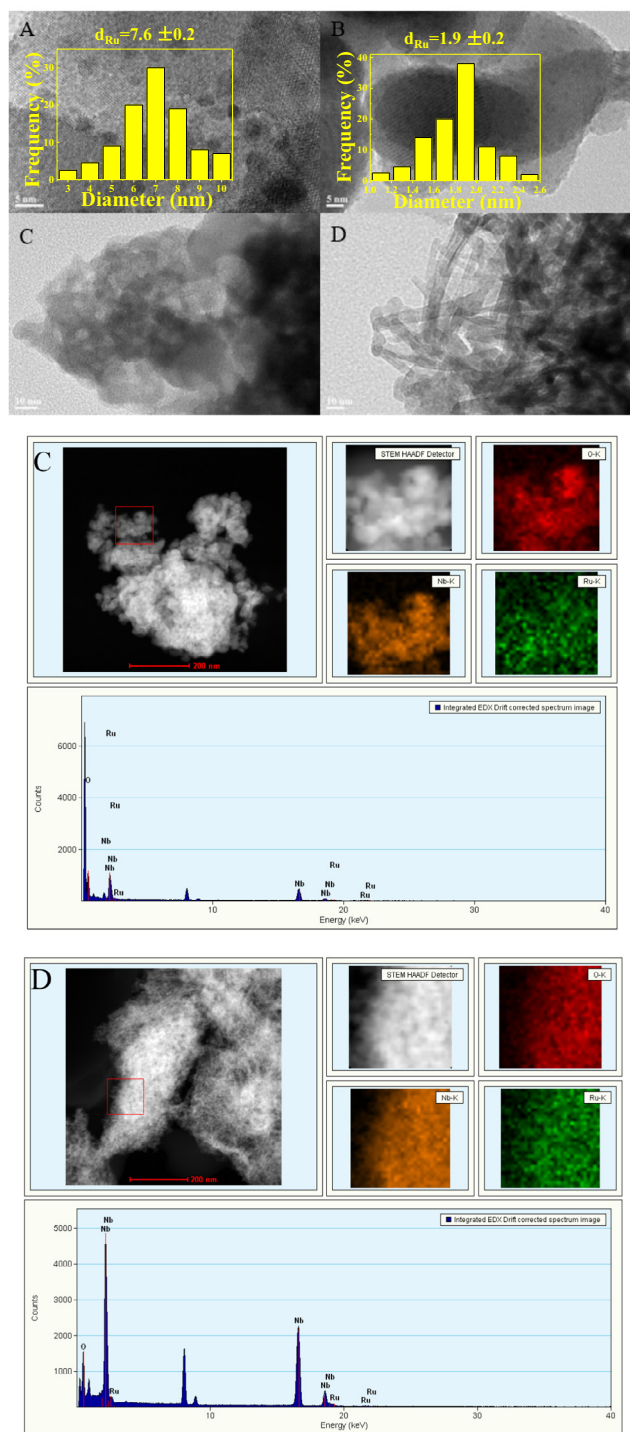


**Fig. 2.** TEM images, particle size distributions and EDS-mapping of various Ru/Nb<sub>2</sub>O<sub>5</sub> (WI) catalysts. (A) Ru/F-Nb<sub>2</sub>O<sub>5</sub>, (B) Ru/H-Nb<sub>2</sub>O<sub>5</sub>, (C) Ru/M-Nb<sub>2</sub>O<sub>5</sub> and (D) Ru/L3-Nb<sub>2</sub>O<sub>5</sub>.

bits higher conversion with the exception of Ru/H-Nb<sub>2</sub>O<sub>5</sub>, indicating that Nb<sub>2</sub>O<sub>5</sub> supports indeed play a significant role in C–O bond activation by excluding the effect of Ru particle size. Interestingly, these four Ru/Nb<sub>2</sub>O<sub>5</sub> (NP) catalysts with 1.2 nm Ru NPs showed a very similar selectivity to toluene (ca. 67%). Whether for conversion or toluene selectivity, Ru/Nb<sub>2</sub>O<sub>5</sub> (WI) shows a better result than that of Ru/Nb<sub>2</sub>O<sub>5</sub> (NP). It is proposed that some active sites of Ru NPs was covered by carbon deposition because ascorbic acid was added as reducing agent during synthesis and solidification

was carried out at 300 °C (N<sub>2</sub>) during Ru/Nb<sub>2</sub>O<sub>5</sub> (NP) preparation, which would result in lower conversion and toluene selectivity.

As the Ru NPs size increase from 1.2 to 1.8 nm and 2.5 nm, the selectivity to toluene decreased dramatically from 64.3% to 52.4% and 37.3%, respectively at similar conversion (30%). These results again suggest that the toluene selectivity has positive relationship with Ru dispersion (Fig. S6) and also is in agreement with the results over Ru/Nb<sub>2</sub>O<sub>5</sub> (WI) and previous report [25,26]. Thus, a conclusion could be given that the layered Nb<sub>2</sub>O<sub>5</sub> supported Ru catalyst showed the best performance in the HDO of 4-methylphenol for both Ru/Nb<sub>2</sub>O<sub>5</sub> (WI) and Ru/Nb<sub>2</sub>O<sub>5</sub> (NP) catalysts. When compared with the reported systems, Ru/L3-Nb<sub>2</sub>O<sub>5</sub> (WI) also showed the best performance (Table S6). Additionally, the HDO of 2- or 3-methylphenol was also carried out over Ru/L3-Nb<sub>2</sub>O<sub>5</sub> (WI) catalyst, which is shown in Table S7. It can be seen that the toluene selectivity remains nearly the same (about 90%) for three substrates, which can be attributed to same Ru particle size. However, the conversion of 2-methylphenol (88.1%) is lower than another two (>99%), it may be due to the steric resistance of 2-methylphenol.

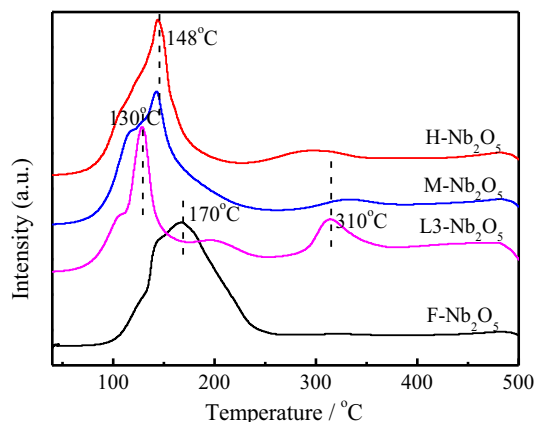
### 3.3. Correlation of the catalytic performance with Nb<sub>2</sub>O<sub>5</sub> surface properties

Raman spectroscopy is very sensitive to the structure and bond order of metal oxides, especially in the region corresponding to metal-oxygen stretching modes [37]. The Raman spectra of various niobium oxides were collected to identify the structure of Nb<sub>2</sub>O<sub>5</sub> and understand the influence of Nb<sub>2</sub>O<sub>5</sub> supports on catalytic performance (Fig. 5A). The broad asymmetric band in the region of 550–800 cm<sup>-1</sup> is assigned to the stretching mode of Nb–O polyhedral, including NbO<sub>6</sub>, NbO<sub>7</sub> and NbO<sub>8</sub>. Compared to the peak at 705 cm<sup>-1</sup> for L3-Nb<sub>2</sub>O<sub>5</sub>, it is shifted to 688 cm<sup>-1</sup> for F-Nb<sub>2</sub>O<sub>5</sub>, M-Nb<sub>2</sub>O<sub>5</sub> and H-Nb<sub>2</sub>O<sub>5</sub>, indicated that the diverse forms of Nb–O polyhedra exhibited some differences on layered Nb<sub>2</sub>O<sub>5</sub>. In addition, a relatively weak peak appears at around 930 cm<sup>-1</sup>, and this peak is regarded as the unsaturated Nb=O surface groups (distorted octahedra) and normally low in concentration [30,37–39]. L3-Nb<sub>2</sub>O<sub>5</sub> has a relatively more intense peak at 930 cm<sup>-1</sup>, suggesting that it has higher concentration of Nb=O surface groups than H-Nb<sub>2</sub>O<sub>5</sub>, M-Nb<sub>2</sub>O<sub>5</sub> and F-Nb<sub>2</sub>O<sub>5</sub> samples. This shows that L3-Nb<sub>2</sub>O<sub>5</sub> with the highest surface area, has the most unsaturated Nb=O surface groups among all four catalysts. Considering the best performance of Ru/L3-Nb<sub>2</sub>O<sub>5</sub> in the HDO of 4-methylphenol, we conclude that the unsaturated surface Nb=O groups play a key role in 4-methylphenol HDO. Additional Raman bands in the low-wavenumber region, 200–400 cm<sup>-1</sup>, are observed in the Nb<sub>2</sub>O<sub>5</sub> spectra, which are the characteristics of bending modes of the Nb–O–Nb linkages.

In order to study the surface chemical environment of the Nb<sub>2</sub>O<sub>5</sub>, the spectra of Nb L<sub>3</sub>-edge X-ray absorption near edge structure spectroscopy (XANES, TEY-mode) were recorded (Fig. 5B). Peaks A and B in the spectra reflected a split of d orbitals originated from the local coordination of Nb<sup>5+</sup>, and the relative peak intensities can be utilized to identify the unit structure as tetrahedral NbO<sub>4</sub> or octahedral NbO<sub>6</sub>, where peak A has a stronger intensity than that of peak B, in the case of octahedral unit. A relative weak peak C sitting at higher energies is attributed to the transitions from 2p<sub>3/2</sub> to the Nb 5s state. For the four Nb<sub>2</sub>O<sub>5</sub> supports, the shape of all spectra was similar to that of LiNbO<sub>3</sub> (octahedral coordination) rather than that of YbNbO<sub>4</sub> (tetrahedral coordination) [40], implying that NbO<sub>6</sub> unit is the major component in these four Nb<sub>2</sub>O<sub>5</sub> support. However, a spectral feature is observed that peaks A and B are more clearly resolved in the spectrum of layered Nb<sub>2</sub>O<sub>5</sub> than that of other three Nb<sub>2</sub>O<sub>5</sub>. Interestingly, the spectral feature of layered Nb<sub>2</sub>O<sub>5</sub> resembles that of NbOx thin films deposited by

**Table 1**  
Physical properties of various Ru/Nb<sub>2</sub>O<sub>5</sub> (WI) catalysts.

Catalysts	Ru loading/wt %	S <sub>BET</sub> /m <sup>2</sup> g <sup>-1</sup>	Ru dispersion/% <sup>a</sup>	CO uptake (μmol/(g of cat))	Ru diameter/nm <sup>c</sup>	Lewis acid (μmol g <sup>-1</sup> ) <sup>d</sup>
Ru/F-Nb <sub>2</sub> O <sub>5</sub>	2.0	15 [16] <sup>b</sup>	4.2	8.3	17.1	127.5
Ru/H-Nb <sub>2</sub> O <sub>5</sub>	1.6	36 [42] <sup>b</sup>	27.0	54.8	2.6	93.7
Ru/M-Nb <sub>2</sub> O <sub>5</sub>	1.7	44 [50] <sup>b</sup>	40.2	79.5	1.8	124.4
Ru/L3-Nb <sub>2</sub> O <sub>5</sub>	1.9	181 [197] <sup>b</sup>	77.0	152.7	0.9	223.6

<sup>a</sup> Ru dispersion determined with CO-pulse titration technique.<sup>b</sup> Data in square brackets is the surface area of Nb<sub>2</sub>O<sub>5</sub>.<sup>c</sup> Ru diameter calculated from CO-pulse adsorption.<sup>d</sup> Lewis acidic amounts is based on Nb<sub>2</sub>O<sub>5</sub> support from Py-FTIR.**Fig. 3.** H<sub>2</sub>-TPR profiles of various Ru/Nb<sub>2</sub>O<sub>5</sub> (WI) catalysts.

Atomic Layer Deposition (ALD), which were amorphous, lacked long-range order, and exhibited the most distortion in the octahedral structure [41]. The structure of distorted octahedral produces

more surface Nb=O species, and exhibits excellent performance in the HDO of 4-methylphenol, which is in accordance with Raman spectrum. A possible surface structures of Nb<sub>2</sub>O<sub>5</sub> was proposed based on Raman and XANES characterizations (Scheme 2).

To further understand the origin of the activity difference over various Ru/Nb<sub>2</sub>O<sub>5</sub> catalysts, the activation behaviors of 4-methylphenol over Ru/L3-Nb<sub>2</sub>O<sub>5</sub>, Ru/M-Nb<sub>2</sub>O<sub>5</sub> catalysts and Ru/H-Nb<sub>2</sub>O<sub>5</sub> were further investigated by Diffuse Reflectance Infrared Fourier Transform Spectroscopy (DRIFTS). For 4-methylphenol, the peak appeared at 1138 cm<sup>-1</sup> region is ascribed to the C<sub>aromatic</sub>-O stretching vibration, and the peaks at 1375 and 1567 cm<sup>-1</sup> are ascribed to the symmetric bending vibration of -CH<sub>3</sub> and skeleton vibration of the aromatic rings, respectively (Fig. S8). Judging by the intensities of 4-methylphenol peaks, it is obvious that the adsorbed amount of 4-methylphenol was much higher over the Ru/L3-Nb<sub>2</sub>O<sub>5</sub> catalyst, in agreement with the trend in the HDO of 4-methylphenol. It is further observed that the bands at 1138 and 1567 cm<sup>-1</sup> are both red shifted for the Ru/L3-Nb<sub>2</sub>O<sub>5</sub> catalyst (Fig. 6A); and the band at 1138 cm<sup>-1</sup> becomes weaker and 1567 cm<sup>-1</sup> becomes stronger with the increases of temperature and time, indicating that the adsorption is activation-required.

**Table 2**  
Conversion and products distribution in the hydrodeoxygenation of 4-methylphenol over various Ru/Nb<sub>2</sub>O<sub>5</sub> (WI) catalysts.<sup>a</sup>

Catalyst	Conv./%	Sel. (%)					Carbon balance/%	TOF <sub>DL</sub> (min <sup>-1</sup> ) <sup>b</sup>	TOF <sub>DS</sub> (min <sup>-1</sup> ) <sup>c</sup>
									
Ru/F-Nb <sub>2</sub> O <sub>5</sub>	21.2	54.9	1.3	2.8	19.0	7.6	96.9	1.5	21.6
Ru/H-Nb <sub>2</sub> O <sub>5</sub>	17.4	62.8	0.7	1.0	15.2	5.8	97.5	1.8	4.0
Ru/M-Nb <sub>2</sub> O <sub>5</sub>	20.9	65.9	0.5	0.7	17.8	7.4	98.4	1.7	3.2
Ru/L3-Nb <sub>2</sub> O <sub>5</sub>	25.1	85.9	0.7	0.9	5.2	2.6	95.5	1.6	0.3

<sup>a</sup> Unless otherwise specified, reaction condition: 0.2 g 4-methylphenol, 0.02 g catalyst and 15 mL H<sub>2</sub>O, 250 °C, 1 h, 0.5 MPa H<sub>2</sub>. The metal loading is 2 wt%.<sup>b</sup> TOF<sub>DL</sub>: the molecule number of the generated toluene per minute/the number of Lewis acid site.<sup>c</sup> TOF<sub>DS</sub>: the molecule number of the generated toluene per minute/the number of surface Ru atoms.**Table 3**  
The hydrodeoxygenation of 4-methylphenol over colloidal Ru NPs loaded Nb<sub>2</sub>O<sub>5</sub> catalysts.<sup>a</sup>

Support	Conv.(%)	Sel. /%					Carbon balance/%	Ru loading/wt % <sup>b</sup>
								
F-Nb <sub>2</sub> O <sub>5</sub>	54.8	67.4	3.1	1.3	18.3	5.8	97.6	1.4
H-Nb <sub>2</sub> O <sub>5</sub>	41.0	66.2	1.8	1.8	22.6	7.7	99.5	1.6
M-Nb <sub>2</sub> O <sub>5</sub>	52.7	66.9	2.6	1.8	20.1	4.7	97.7	1.5
L3-Nb <sub>2</sub> O <sub>5</sub>	72.3	68.1	2.9	1.2	17.4	2.6	98.4	1.5

<sup>a</sup> Unless otherwise specified, reaction condition: 0.2 g 4-methylphenol, 0.04 g catalyst and 15 mL H<sub>2</sub>O, 250 °C, 2 h, 0.5 MPa H<sub>2</sub>. The size of colloidal Ru NPs are 1.2 nm and theoretical loading is 2 wt%.<sup>b</sup> Determined by ICP.

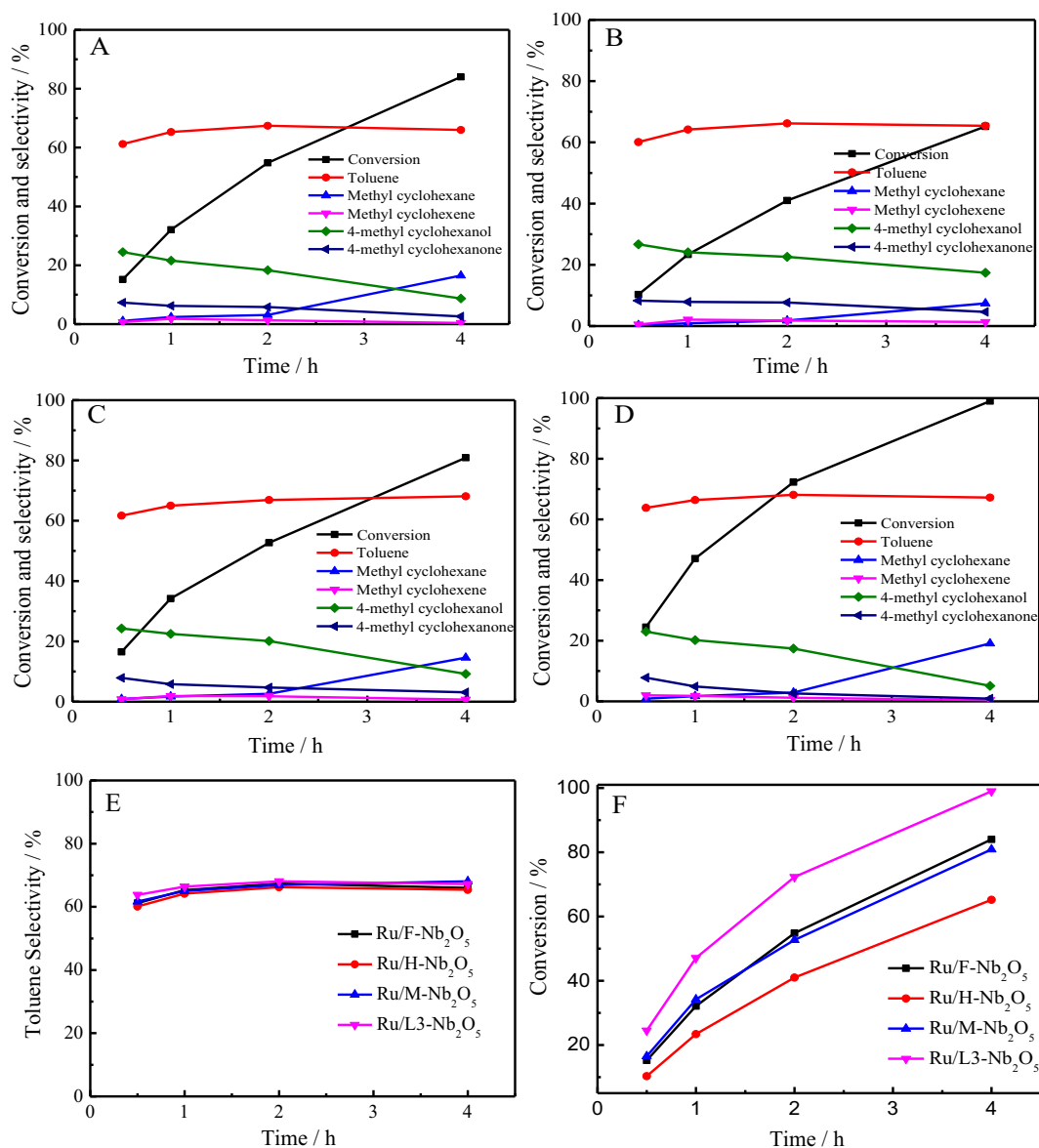


**Fig. 4.** Product distributions for the conversion of 4-methylphenol in the time courses over (A) Ru/F-Nb<sub>2</sub>O<sub>5</sub> (NP, 1.2 nm), (B) Ru/H-Nb<sub>2</sub>O<sub>5</sub> (NP, 1.2 nm), (C) Ru/M-Nb<sub>2</sub>O<sub>5</sub> (NP, 1.2 nm), (D) Ru/L3-Nb<sub>2</sub>O<sub>5</sub> (NP, 1.2 nm) catalyst. (E) Toluene selectivity on four catalysts. (F) Conversion of 4-methylphenol on four catalysts.

The red shift of the  $C_{\text{aromatic}}-\text{O}$  bonds was due to the strong adsorption of  $C_{\text{aromatic}}-\text{O}$  bonds on NbO<sub>x</sub> species, which leads to its weakness. The strong adsorption of  $C_{\text{aromatic}}-\text{O}$  bonds further makes electrons on benzene rings delocalized, leading to the red-shift. However, there is little peak shift for the Ru/M-Nb<sub>2</sub>O<sub>5</sub> catalyst (Fig. 6B), in agreement with its poorer activity than that of Ru/L3-Nb<sub>2</sub>O<sub>5</sub> catalyst. Over Ru/H-Nb<sub>2</sub>O<sub>5</sub> catalyst (Fig. S7), the band at 1375 cm<sup>-1</sup> (symmetric bending vibration of -CH<sub>3</sub>) disappeared and a new band at 1450 cm<sup>-1</sup> ascribed to the asymmetric bending vibration of -CH<sub>3</sub> is observed. We inferred that the difference on vibration of -CH<sub>3</sub> in DRIFTS leads to the low conversion over Ru/H-Nb<sub>2</sub>O<sub>5</sub> catalyst, but the selectivity to toluene is the same, because it depends on Ru particle size. All these results confirm that the activation of  $C_{\text{aromatic}}-\text{O}$  bonds is very important and it is most effective in Ru/L3-Nb<sub>2</sub>O<sub>5</sub> catalyst.

Furthermore, we carried out Py-FTIR experiments, calculated the Brønsted and Lewis acids of four Nb<sub>2</sub>O<sub>5</sub> and correlated the conversion of 4-methylphenol with the Lewis acidic amount over four Ru/Nb<sub>2</sub>O<sub>5</sub> (NP, 1.2 nm) catalysts. It is shown that the amount of

Brønsted acid was low and that of Lewis acid was high, indicating niobia is Lewis acid-dominated (Table S8). The Lewis acidic amounts of four samples decrease in the following order: L3-Nb<sub>2</sub>O<sub>5</sub> (223.6 μmol g<sup>-1</sup>) > M-Nb<sub>2</sub>O<sub>5</sub> (124.4 μmol g<sup>-1</sup>) ≈ F-Nb<sub>2</sub>O<sub>5</sub> (127.5 μmol g<sup>-1</sup>) > H-Nb<sub>2</sub>O<sub>5</sub> (93.7 μmol g<sup>-1</sup>), well in accordance with the order of conversion over four Ru/Nb<sub>2</sub>O<sub>5</sub> (NP, 1.2 nm) catalysts. The plot of conversion vs. Lewis acid shows a nearly linear relationship (Fig. 7). Furthermore, the TOF values were calculated based on Lewis acid sites for DDO route (toluene production), denoted as TOF<sub>DL</sub>, which is nearly constant in four catalysts, indicating that Lewis acid sites (unsaturated NbO<sub>x</sub> species) are active sites for toluene formation.

In order to confirm the conclusion, the TOF values based on Lewis acid sites and surface Ru atoms for DDO route (toluene production) were also calculated over Ru/Nb<sub>2</sub>O<sub>5</sub> (WI) catalysts, which are denoted as TOF<sub>DL</sub> and TOF<sub>DS</sub>, respectively. All data were collected in Table 2. It can be seen that the TOF<sub>DL</sub> values are nearly constant based on toluene production, confirming again that Lewis acid sites (unsaturated NbO<sub>x</sub> species) are the catalytic sites for

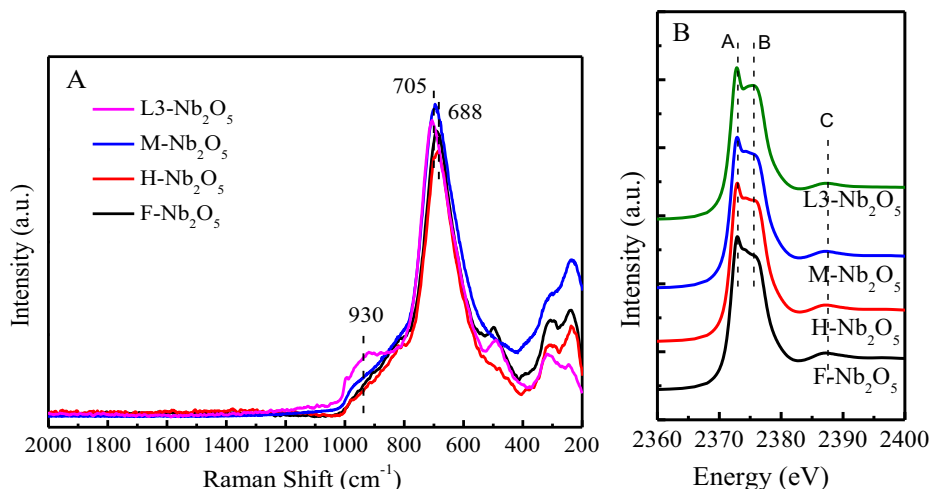
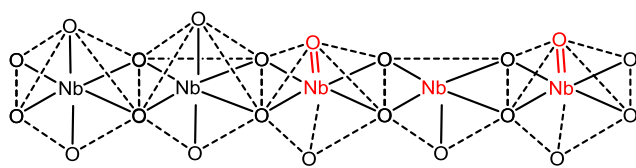


Fig. 5. Raman spectra of various  $\text{Nb}_2\text{O}_5$  (A) and Nb  $L_3$ -edge XANES spectra of  $\text{Nb}_2\text{O}_5$  in TEY mode. (B).



Scheme 2. Possible surface structures of  $\text{Nb}_2\text{O}_5$ .

toluene production and there is no intrinsic difference on unsaturated  $\text{NbO}_x$  species over four catalysts. While the  $\text{TOF}_{\text{DS}}$  values based on surface Ru atoms are so different, meaning Ru nanoparticles would not be the key active sites for toluene production.

#### 3.4. Design of a more active Ru/ $\text{Nb}_2\text{O}_5$ catalyst

Usually, it is considered that the conditions during hydrothermal synthesis can change the phases and degree of crystallization of metal oxides [42]. In order to design a more effective catalyst for the production of aromatic hydrocarbons through HDO of lignin, a short hydrothermal time (1 day) was taken to prepare another layered  $\text{Nb}_2\text{O}_5$ , denoted as L1- $\text{Nb}_2\text{O}_5$  and its physical properties were present in Table S8. We hope that L1- $\text{Nb}_2\text{O}_5$  has lower crystallinity and more surface  $\text{Nb}=\text{O}$  groups than that of L3- $\text{Nb}_2\text{O}_5$ , thus has a better performance for the HDO of lignin and lignin model compound. XANES spectra in Fig. 8A confirmed that peaks A and B are clearly resolved in the spectrum of L1- $\text{Nb}_2\text{O}_5$ , similar to that

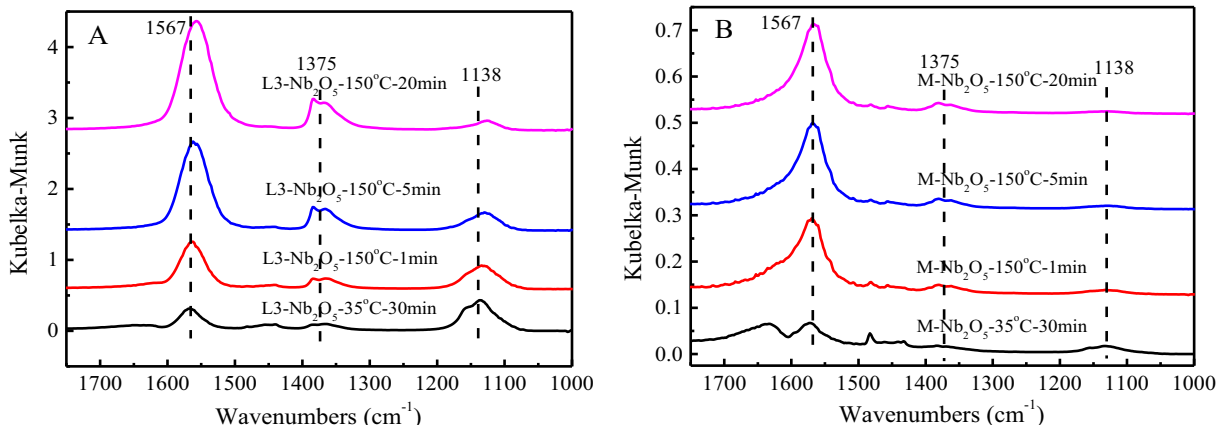


Fig. 6. DRIFTS spectra obtained over (A) Ru/L3- $\text{Nb}_2\text{O}_5$  and (B) Ru/M- $\text{Nb}_2\text{O}_5$ .

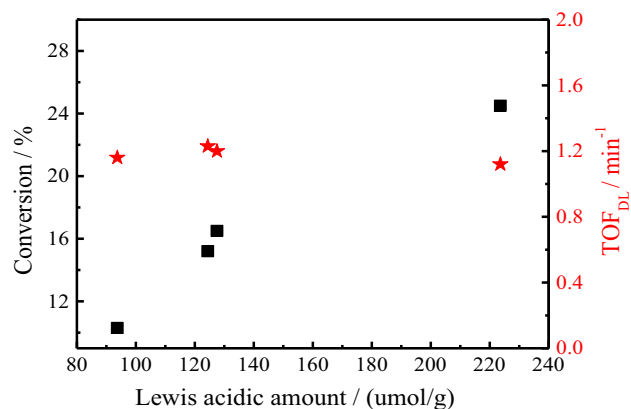


Fig. 7. 4-methylphenol conversion and  $\text{TOF}_{\text{DL}}$  vs Lewis acidic amount over four Ru/ $\text{Nb}_2\text{O}_5$  (NP, 1.2 nm) catalysts.

of the L3- $\text{Nb}_2\text{O}_5$ , indicating that a large amount of unsaturated  $\text{NbO}_x$  sites also existed on the surface of L1- $\text{Nb}_2\text{O}_5$ . In addition, Raman spectra (Fig. 8B) show the higher intensity of peak at  $930\text{ cm}^{-1}$  over L1- $\text{Nb}_2\text{O}_5$  than that over L3- $\text{Nb}_2\text{O}_5$ , confirming that more  $\text{Nb}=\text{O}$  groups existed on L1- $\text{Nb}_2\text{O}_5$  surface due to the short hydrothermal treatment.

Furthermore, the HDO of 4-methylphenol was conducted to compare the performances of Ru/L1- $\text{Nb}_2\text{O}_5$  and Ru/L3- $\text{Nb}_2\text{O}_5$  (WI) catalysts, and the results were shown in Fig. 9. As expected, the

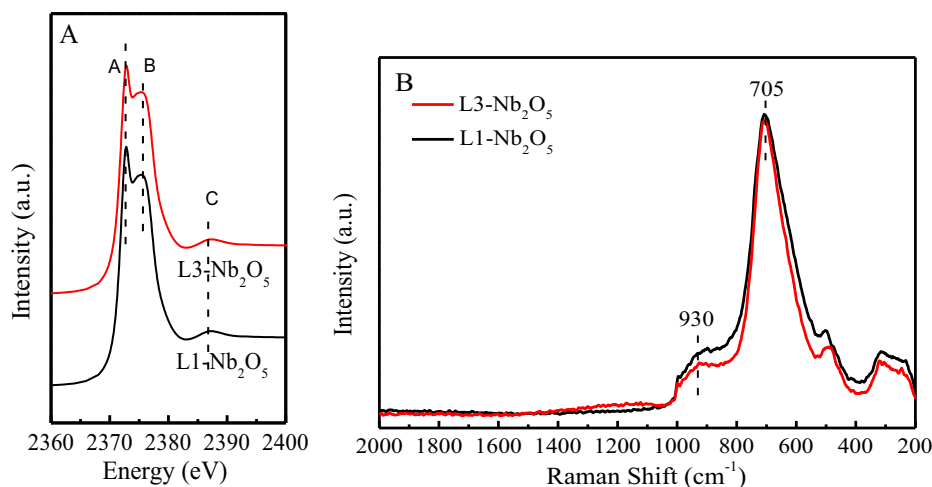


Fig. 8. (A) Nb L<sub>3</sub>-edge XANES spectra of L1-Nb<sub>2</sub>O<sub>5</sub> and L3-Nb<sub>2</sub>O<sub>5</sub> in TEY mode. (B) Raman spectra of L1-Nb<sub>2</sub>O<sub>5</sub> and L3-Nb<sub>2</sub>O<sub>5</sub>.

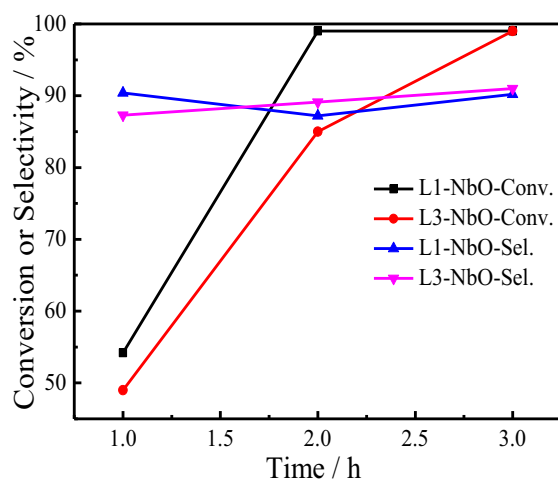


Fig. 9. Activity results of 2% Ru/L1-Nb<sub>2</sub>O<sub>5</sub> (WI) and 2% Ru/L3-Nb<sub>2</sub>O<sub>5</sub> (WI) as a function of time. Reaction condition: substrate (0.2 g), catalyst (0.04 g), deionized water (15 mL), 250 °C and initial H<sub>2</sub> pressure of 0.5 MPa.

conversions of 4-methylphenol over Ru/L1-Nb<sub>2</sub>O<sub>5</sub> is generally higher than that over Ru/L3-Nb<sub>2</sub>O<sub>5</sub> catalyst at all reaction times although the selectivity to toluene is similar (90%), confirming the key role of unsaturated NbO<sub>x</sub> species (surface Nb=O groups) in HDO of 4-methylphenol.

Table 4

Main product selectivity from hydrodeoxygenation of enzymatic lignin over layered Ru/Nb<sub>2</sub>O<sub>5</sub> (WI) catalysts.<sup>a</sup>

Catalysts	Mole yield of C <sub>7</sub> ~C <sub>9</sub> hydrocarbons <sup>d</sup> /%						Sum of C <sub>7</sub> ~C <sub>9</sub> hydrocarbons/mol%	Select. to arenes/mol%
								
L1-Nb <sub>2</sub> O <sub>5</sub>	1.6	7.8	2.4	26.3	4.0	11.4	53.6	85.0
L3-Nb <sub>2</sub> O <sub>5</sub>	1.1	6.7	1.6	24.0	3.0	9.2	45.5	86.5
M-Nb <sub>2</sub> O <sub>5</sub>	0.8	5.0	4.3	16.1	1.6	3.8	31.6	78.7
L1-Nb <sub>2</sub> O <sub>5</sub> <sup>b</sup>	2.5	12.1	6.9	53.0	3.3	21.6	99.4	87.3
L1-Nb <sub>2</sub> O <sub>5</sub> <sup>c</sup>	0.9	16.0	3.0	62.0	0.9	17.3	99.6	94.8

<sup>a</sup> Reaction condition: 0.1 g enzymatic lignin, 0.2 g catalyst, 10 mL H<sub>2</sub>O, 5 mL cyclohexane, 250 °C, 10 h, initial H<sub>2</sub> pressure of 0.7 MPa H<sub>2</sub>.

<sup>b</sup> Reaction condition: the same as <sup>a</sup> with the exception of reaction time, 20 h here.

<sup>c</sup> Reaction condition: the same as <sup>b</sup> with the exception of solvent, 15 mL H<sub>2</sub>O here.

<sup>d</sup> The yields of products are calculated by using the equation:  $Y_{\text{product}} = n_{\text{product}}/n_{\text{total theoretical monomer}}$ , the molar quantity of the total theoretical monomer in 0.1 g enzymatic lignin is 0.145 mmol.

Moreover, the HDO of enzymatic lignin was conducted over Ru/L1-Nb<sub>2</sub>O<sub>5</sub> (WI) catalyst at 250 °C for 10 h in the mixed solvent (H<sub>2</sub>O and cyclohexane) and compared with that of Ru/L3-Nb<sub>2</sub>O<sub>5</sub> (WI) and Ru/M-Nb<sub>2</sub>O<sub>5</sub> (WI) (Table 4). It can be found that the yield of hydrocarbons (53.6%, based on the monomers) over Ru/L1-Nb<sub>2</sub>O<sub>5</sub> is high than that over Ru/L3-Nb<sub>2</sub>O<sub>5</sub> (45.5%), with the similar selectivity to aromatic hydrocarbons (ca. 86%); while over Ru/M-Nb<sub>2</sub>O<sub>5</sub> (WI) catalyst, the yield of hydrocarbons (31.6%) and selectivity to aromatic hydrocarbons (76.8%) are both lower. All these results agreed well with those of 4-methylphenol hydrodeoxygenation. By extending the reaction time to 20 h, the yield of hydrocarbons reached 99.4% with the similar selectivity. For Ru/L1-Nb<sub>2</sub>O<sub>5</sub> catalyst, the selectivity to arenes is much higher than that over Ru/M-Nb<sub>2</sub>O<sub>5</sub> for organosolv lignin (ca. 70%) [21] and enzymatic lignin (76.8%), further confirmed that Nb<sub>2</sub>O<sub>5</sub> with more unsaturated Nb=O species has high activity. When the reaction was carried out in aqueous phase, the selectivity to arenes can be further improved (94.8%, Table 4) because the aqueous phase can enhance the separation of arenes from solvent and prevent further hydrogenation of arenes. GC profile is given to corroborate the results (Fig. S10).

### 3.5. Reusability of Ru/L1-Nb<sub>2</sub>O<sub>5</sub> catalyst in the HDO of enzymatic lignin

The test of the reusability of Ru/L1-Nb<sub>2</sub>O<sub>5</sub> catalyst was conducted in a batch reactor for three successive times and the results are illustrated in Fig. 10. After each reaction, the “used” catalyst is washed with water and tetrahydrofuran, then dried under vacuum

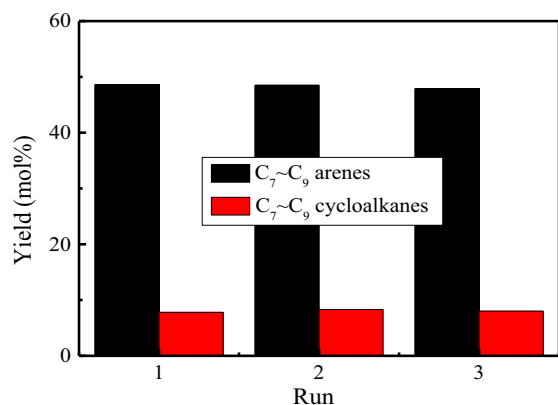


**Fig. 10.** Products distribution in three successive runs during the HDO of enzymatic lignin over Ru/L1-Nb<sub>2</sub>O<sub>5</sub> catalyst. Reaction conditions: enzymatic lignin 0.1 g, catalyst 0.2 g, 10 mL H<sub>2</sub>O, 5 mL cyclohexane, 250 °C, H<sub>2</sub> 0.7 MPa, 20 h.

(50 °C), and directly recharged for the next run. No significant deactivation was observed even after three successive runs. XRD re-measurement showed that there was no change of the layered structure (Fig. S11) and TEM image showed that Ru nanoparticles did not aggregated obviously after the successive 4 runs (Fig. S12). All these results (Table S9) indicate the good stability of Ru/L1-Nb<sub>2</sub>O<sub>5</sub> catalyst, in agreement with previous report [21].

#### 4. Conclusion

In summary, four Nb<sub>2</sub>O<sub>5</sub> supports with different morphologies were used as support to prepare Ru/Nb<sub>2</sub>O<sub>5</sub> (WI) catalysts by wetness impregnation. The Nb<sub>2</sub>O<sub>5</sub> with different morphologies has different surface area, leading to different unsaturated NbO<sub>x</sub> sites and Ru dispersion, and further affected the catalytic activity and toluene selectivity in the HDO of 4-methylphenol. The layered Nb<sub>2</sub>O<sub>5</sub> support has the highest surface area and Ru dispersion and shows the best performance. Its selectivity to toluene was highest (90%) with a full 4-methylphenol conversion after reaction at 250 °C for 3 h, much high than those over other catalysts. Ru colloids with uniform nanoparticles size was pre-synthesized and loaded on these four Nb<sub>2</sub>O<sub>5</sub> supports to investigate the intrinsic effect of Nb<sub>2</sub>O<sub>5</sub> and it is found that the layered Ru/Nb<sub>2</sub>O<sub>5</sub> (NP) catalyst showed best performance among all catalysts with different Nb<sub>2</sub>O<sub>5</sub> supports but the same Ru NPs size. In addition, it was proved that the toluene selectivity was dependent on the size of Ru particles and smaller Ru NPs showed higher selectivity to aromatic hydrocarbons. Raman spectroscopy and XANES show that layered Nb<sub>2</sub>O<sub>5</sub> has more unsaturated surface Nb=O groups, which play a key role in the HDO of 4-methylphenol. DRIFTS and Py-FTIR further confirmed that unsaturated NbO<sub>x</sub> sites on Ru/L3-Nb<sub>2</sub>O<sub>5</sub> catalyst possess strong adsorption and activation ability for 4-methylphenol. Furthermore, a Ru/L1-Nb<sub>2</sub>O<sub>5</sub>(WI) catalyst with more unsaturated NbO<sub>x</sub> species was designed and prepared, which exhibited an excellent performance in the HDO of enzymatic lignin, with its selectivity to aromatic hydrocarbons reaching up to 94.8% in aqueous phase.

#### Acknowledgements

This work was supported financially by the NSFC of China (No. 91545103, 21603072, 21832002, 21872050, 21808063), the Fundamental Research Funds for the Central Universities

(222201718003) and the Science and Technology Commission of Shanghai Municipality (10dz2220500).

#### Appendix A. Supplementary material

Supplementary data to this article can be found online at <https://doi.org/10.1016/j.jcat.2019.05.007>.

#### References

- [1] J. Zakzeski, P.C. Bruijninx, A.L. Jongerijs, B.M. Weckhuysen, *Chem. Rev.* 110 (2010) 3552–3599.
- [2] J.S. Luterbacher, D.M. Alonso, J.A. Dumesic, *Green Chem.* 16 (2014) 4816–4838.
- [3] A.J. Ragauskas, G.T. Beckham, M.J. Bidy, R. Chandra, F. Chen, M.F. Davis, B.H. Davison, R.A. Dixon, P. Gilna, M. Keller, P. Langan, A.K. Naskar, J.N. Saddler, T.J. Tschaplinski, G.A. Tuskan, C.E. Wyman, *Science* 344 (2014) 709–720.
- [4] P. Azadi, O.R. Inderwildi, R. Farnood, D.A. King, *Renew. Sust. Energ. Rev.* 21 (2013) 506–523.
- [5] C. Li, X. Zhao, A. Wang, G.W. Huber, T. Zhang, *Chem. Rev.* 115 (2015) 11559–11624.
- [6] X. Wang, R. Rinaldi, *Energy Environ. Sci.* 5 (2012) 8244–8260.
- [7] Q. Song, F. Wang, J. Cai, Y. Wang, J. Zhang, W. Yu, J. Xu, *Energy Environ. Sci.* 6 (2013) 994–1007.
- [8] A. Rahimi, A. Ulbrich, J.J. Coon, S.S. Stahl, *Nature* 515 (2014) 249–252.
- [9] P.J. Deuss, M. Scott, F. Tran, N.J. Westwood, J.G. de Vries, K. Barta, *J. Am. Chem. Soc.* 137 (2015) 7456–7467.
- [10] J. Kong, M. He, J.A. Lercher, C. Zhao, *Chem. Commun.* 5 (2015) 17580–17583.
- [11] T. Parsell, S. Yohe, J. Degenstein, T. Jarrell, I. Klein, E. Gencer, B. Hewetson, M. Hurt, J.I. Kim, H. Choudhari, B. Saha, R. Meilan, N. Mosier, F. Ribeiro, W.N. Delgass, C. Chapple, H.I. Kenttämä, R. Agrawal, M.M. Abu-Omar, *Green Chem.* 17 (2015) 1492–1499.
- [12] H. Wang, H. Ruan, H. Pei, H. Wang, X. Chen, M.P. Tucker, J.R. Cort, B. Yang, *Green Chem.* 17 (2015) 5131–5135.
- [13] S. Van den Bosch, W. Schutyser, R. Vanholme, T. Driessen, S.F. Koelewijn, T. Renders, B. De Meester, W.J.J. Huijgen, W. Dehaen, C.M. Courtin, B. Lagrain, W. Boerjan, B.F. Sels, *Energy Environ. Sci.* 8 (2015) 1748–1763.
- [14] X.M. Huang, O.M.M. Gonzalez, J.D. Zhu, T.I. Korányi, M.D. Boot, E.J. Hensen, *Green Chem.* 19 (2016) 175–187.
- [15] L. Shuai, M.T. Amiri, Y.M. Questell-Santiago, F. Héroguel, Y.D. Li, H. Kim, R. Meilan, C. Chapple, J. Ralph, J.S. Luterbacher, *Science* 354 (2016) 329–333.
- [16] Z. Sun, G. Bottari, A. Afanasenko, M.C.A. Stuart, P.J. Deuss, B. Fridrich, K. Barta, *Nat. Catal.* 1 (2018) 82–92.
- [17] F. Chen, N. Li, A.Q. Wang, T. Zhang, *Chem. Commun.* 51 (2015) (1879) 11876–11881.
- [18] S. Echeandia, P.L. Arias, V.L. Barrio, B. Pawelec, J.L.G. Fierro, *Appl. Catal. B-Environ.* 101 (2010) 1–12.
- [19] X. Wang, R. Rinaldi, *Angew. Chem. Int. Ed.* 52 (2013) 11499–11503.
- [20] B. Feng, H. Kobayashi, H. Ohta, A. Fukuoka, *J. Mol. Catal. A-Chem.* 388 (2014) 41–46.
- [21] Y. Shao, Q. Xia, L. Dong, X. Liu, X. Han, S.F. Parker, Y. Cheng, L.L. Daemen, A.J. Ramirez-Cuesta, S. Yang, Y. Wang, *Nat. Commun.* 8 (2017) 16104–16112.
- [22] T. Guo, Q. Xia, Y. Shao, X. Liu, Y. Wang, *Appl. Catal. A-Gen.* 547 (2017) 30–36.
- [23] A. Tuxen, S. Careno, M. Chintapalli, C.H. Chuang, C. Escudero, E. Pach, P. Jiang, F. Borondics, B. Beberwyck, A.P. Alivisatos, G. Thornton, W.F. Pong, J. Guo, R. Perez, F. Besenbacher, M. Salmeron, *J. Am. Chem. Soc.* 135 (2013) 2273–2278.
- [24] W. Chen, J. Ji, X. Feng, X. Duan, G. Qian, P. Li, X. Zhou, D. Chen, W. Yuan, *J. Am. Chem. Soc.* 136 (2014) 16736–16739.
- [25] C. Newman, X. Zhou, B. Goundie, I.T. Ghamson, R.A. Pollock, Z. Ross, M.C. Wheeler, R.W. Meulenber, R.N. Austin, B.G. Frederick, *Appl. Catal. A-Gen.* 477 (2014) 64–74.
- [26] L. Dong, L. Yin, Q. Xia, X. Liu, X. Gong, Y. Wang, *Catal. Sci. Technol.* 8 (2018) 735–745.
- [27] M. Raula, M.H. Rashid, T.K. Paira, E. Dinda, T.K. Mandal, *Langmuir* 26 (2010) 8769–8782.
- [28] Z. Qiao, Z. Wu, S. Dai, *ChemSusChem* 6 (2013) 1821–1833.
- [29] P.M. de Souza, R.C. Rabelo-Neto, L.E.P. Borges, G. Jacobs, B.H. Davis, U.M. Graham, D.E. Resasco, F.B. Noronha, *ACS Catal.* 5 (2015) 7385–7398.
- [30] H.T. Kreissl, M.M.J. Li, Y.K. Peng, K. Nakagawa, T.J.N. Hooper, J.V. Hanna, A. Shepherd, T.S. Wu, Y.L. Soo, S.C.E. Tsang, *J. Am. Chem. Soc.* 139 (2017) 12670–12680.
- [31] Y. Zhang, J. Wang, J. Ren, X. Liu, X. Li, Y. Xia, G. Lu, Y. Wang, *Catal. Sci. Technol.* 2 (2012) 2485–2491.
- [32] W. Fan, Q. Zhang, W. Deng, Y. Wang, *Chem. Mat.* 25 (2013) 3277–3287.
- [33] L. Kong, C. Zhang, J. Wang, W. Qiao, L. Ling, D. Long, *Sci. Rep.* 6 (2016) 21177.
- [34] T. Murayama, J. Chen, J. Hirata, K. Matsumoto, W. Ueda, *Catal. Sci. Technol.* 4 (2014) 4250–4257.
- [35] P. Sun, X. Long, H. He, C. Xia, F. Li, *ChemSusChem* 6 (2013) 2190–2197.
- [36] S. Chai, H. Wang, Y. Liang, B. Xu, *J. Catal.* 250 (2007) 342–349.
- [37] J.M. Jehng, I.E. Wachs, *Chem. Mat.* 3 (1991) 100–107.

- [38] N.T. do Prado, T.E. Souza, A.R.T. Machado, P.P. Souza, R.S. Monteiro, L.C.A. Oliveira, J. Mol. Catal. A-Chem. 422 (2016) 23–34.
- [39] H.T. Kreissl, K. Nakagawa, Y.K. Peng, Y. Koito, J. Zheng, S.C.E. Tsang, J. Catal. 338 (2016) 329–339.
- [40] Y. Kubouchi, S. Hayakawa, H. Namatame, T. Hirokawa, X-Ray Spectrom. 41 (2012) 259–263.
- [41] B. Wang, Y. Zhao, M.N. Banis, Q. Sun, K.R. Adair, R. Li, T.K. Sham, X. Sun, ACS Appl Mater. Interfaces 10 (2018) 1654–1661.
- [42] Y.Q. Song, H.M. Liu, D.H. He, Energy Fuels 24 (2010) 2817–2824.